

Open-RadVLAD: Fast and Robust Radar Place Recognition

Matthew Gadd and Paul Newman
Mobile Robotics Group, University of Oxford

✉ mattgadd@robots.ox.ac.uk 🌐 github.com/mttgdd/open-radvlad

Abstract—Radar place recognition often involves encoding a live scan as a vector and matching this vector to a database in order to recognise that the vehicle is in a location that it has visited before. Radar is inherently robust to lighting or weather conditions, but place recognition with this sensor is still affected by: (1) viewpoint variation, i.e. translation and rotation, (2) sensor artefacts or “noises”. For 360° scanning radar, rotation is readily dealt with by in some way aggregating across azimuths. Also, we argue in this work that it is more critical to deal with the richness and informativeness of representation than it is to deal with translational invariance – particularly in urban driving where vehicles predominantly follow the same lane when repeating a route. In our method, for computational efficiency, we use only the polar representation. For partial translation invariance, we use only a one-dimensional Fourier Transform along radial returns. As the original radar signal is in the form of received power in discretised range bins, we also show experimentally that taking a radial Fourier Transform in this way and matching based on spatial frequencies present in the power signal leads to better performance – leading to a 7% to 8% improvement in localisation success (Section IV and Table II). We also achieve rotational invariance and a very discriminative descriptor space by building a vector of locally aggregated descriptors (VLAD). Our method is more comprehensively tested than all prior radar place recognition work – over an exhaustive combination of all 870 pairs of trajectories from 30 *Oxford Radar RobotCar Dataset* sequences (each ≈ 10 km), with a frequency-modulated continuous-wave (FMCW) radar. Code and detailed results are provided at github.com/mttgdd/open-radvlad, as an open implementation and benchmark for future work in this area. We achieve a mean of 89.35% and median of 91.52% in $\text{Recall}@1$, outstripping the mean of 68.56% and median of 69.55% for the only other open implementation, *RaPlace*, and at a fraction of its computational cost (relying on fewer integral transforms e.g. Radon, Fourier, and inverse Fourier).

Index Terms—Radar, Localisation, Place Recognition, Autonomous Vehicles, Robotics

I. INTRODUCTION

For autonomous vehicles to drive in a safe way even in the face of challenging illumination or weather conditions very robust sensing is required. Thus, the interest in scanning frequency-modulated continuous-wave radar for place recognition and localisation. However, radar place recognition is not an especially mature research area – there are few open-source implementations and no exhaustive evaluations. Therefore, in this work, our principal contributions are:

- 1) A novel **simplification** of recent work using integral transform techniques – using only a single forward Fourier Transform, with better place recognition **performance** and with much faster computation,
- 2) An **exhaustive evaluation** over the *Oxford Radar RobotCar Dataset* – the largest such evaluation to date, and

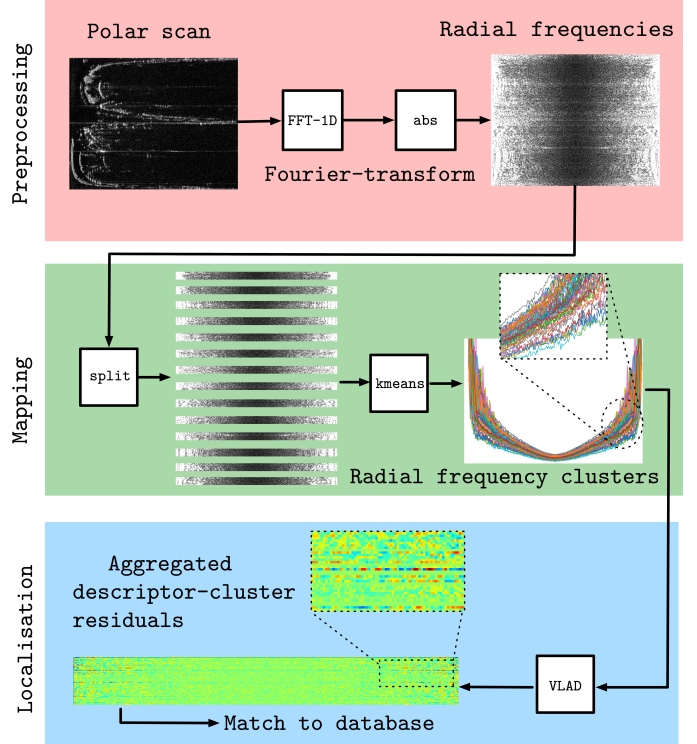


Fig. 1: *Open-RadVLAD* system overview. For a degree of robustness, we take the 1D Fourier Transform of the radial returns. Clustering these radial frequency responses is not specific to azimuth order and so gives us rotational invariance. Therefore, we apply a “vector of locally aggregated descriptors” (VLAD) as an informative scan descriptor with the residuals of query radial frequency responses to those cluster centres.

- 3) An **open implementation**, to serve as a platform for future research.

Figure 1 gives an overview of our system. For background, place recognition can be performed by matching a vector representation of radar scans to vectors from previously visited places (indicated by Match to database). This paper is about *engineering good representations* – with incorrect matches “far away” and correct matches “close by” in that vector space.

II. RELATED WORK

Several recent radar datasets use the same radar class – from the same manufacturer¹ – as used in our work, including

¹*Navtech Radar*: navtechradar.com

the *Oxford Radar RobotCar Dataset* [1] by Barnes *et al*, *MulRan* [2] by Kim *et al*, *RADIATE* [3] by Sheeny *et al*. The *Oxford Radar RobotCar Dataset* [1] is purely urban and features many repeat traversals, useful in investigating place recognition.

Radar place recognition has been explored in [4], [5], [6], [7], [8], [9], [10], [11], [12], [13]. This has included simultaneous localisation and mapping techniques [10], [11] methods for learning to vectorise radar scans with neural networks in [4], [5], [9], [7], [8], [13] and also non-learned methods [2], [6], [12].

The most relevant to our work is *RaPlace* by Jang *et al* [12] as originally applied to LiDAR place recognition in *RING* by Lu *et al* in [14]. In these works, a Radon Transform [15] on the Cartesian scan gives a Sinogram, and a Fourier Transform of this Sinogram gives a descriptor which is totally insensitive to translation of the Cartesian scan, and shifts circularly under rotation of the Cartesian scan. Then, circular cross-correlation is used to measure the similarity between descriptors in a rotationally-invariant way. This circular cross-correlation itself involves two Fourier Transforms and an inverse Fourier Transform.

Our experimental results in Section V indicate that a much greater impact on localisation performance is available by focusing on the richness of the vector representation rather than translation invariance. We do, however, as detailed further in Section III below, use the Fourier Transform directly on polar radar returns (rather than a Sinogram obtained from the Cartesian scan which itself is obtained from the polar scan).

III. METHOD

As shown in the top left of Figure 1 by `Polar scan`, we start with range-bearing arrays $f(r, \theta) \in \mathbb{R}^{W \times H}$ where W is the number of range bins r (horizontal axis) and H is the number of discrete azimuths θ (vertical axis).

Then, we then take the 1D Discrete Fourier Transform along the radial dimension

$$\hat{f}(\rho, \theta) = \sum_{r=0}^{W-1} f(r, \theta) e^{-\frac{i2\pi}{W} \rho r} \quad (1)$$

giving radial frequency responses along each heading. Although as mentioned in Section I these radial returns are themselves powers, the use of the Fourier Transform with the *Navtech* class of radar sensor (Section IV) has been shown to be effective in e.g. [16] – and similarly for the related Fourier Mellin Transform (FMT) in [17] – and is proved in Section IV to give an important boost to place recognition performance. We specifically use the magnitude of this complex number $\hat{f}_{\text{abs}}(\rho, \theta) = |\hat{f}(\rho, \theta)|$. These steps are shown as `FFT-1D` and `abs` in Figure 1. Each of these radial frequency response magnitudes is a W -dimensional vector $\hat{f}_{\text{abs}}(\rho, \theta_j)$ specific to a heading θ_j , shown after the `split` in Figure 1.

Now, with more detail below, localisation consists of matching a sequence of query scans to a sequence of reference scans – the latter being referred to as a “map”. We now take all radial

frequency responses from all scans in a map trajectory² (or “experience”) and find cluster centres $C = \{c_1, c_2, \dots, c_k\}$ where each $c_i \in \mathbb{R}^W$ is in the space formed by all \hat{f}_{abs} from all azimuths from all scans in the map. Examples of these radial frequency clusters are shown in Figure 1 (middle, green).

Now, as in Equation (3) below, to find matches between the query experience and map experience, we convert polar map scans as well as polar query scans into some vector representation between which we can compute distances. For this, we use the vector of locally aggregated descriptors [18]. Here, each contiguous section of the “vector of locally aggregated descriptors” (VLAD) descriptor \mathbf{v}_i is computed as the sum of residuals from every radial frequency response which has its nearest cluster (written `nn` in Equation (2)) the centre corresponding to that section, as per

$$\mathbf{v}_i = \sum_{\mathbf{x}_j | \text{nn}(\mathbf{x}_j) = c_i} (\mathbf{x}_j - c_i), \quad \mathbf{x}_j = \hat{f}_{\text{abs}}(\rho, \theta_j) \quad (2)$$

and the full VLAD descriptor \mathbf{v} is found by concatenating \mathbf{v}_i for all c_i . An example is shown in Figure 1 (bottom, blue).

With map VLAD descriptors \mathbf{v}^j at places indexed by j and query VLAD descriptor \mathbf{w} , localisation can then be stated as

$$j^* = \operatorname{argmin}_j \|\mathbf{w} - \mathbf{v}^j\|_2^2 \quad (3)$$

where we decide that we are in place j^* given that the descriptor for that place is closest to our query descriptor (i.e. “place recognition”).

Note that we may also accept the N nearest neighbours as a range of j^* values for putative localisation candidates, as we do in our experiments in Sections IV and V. With more than 1 candidate, it is often expected as in e.g. [2] that some downstream pose refinement module disambiguates them and chooses the correct result, with hierarchical interaction between the “place recognition” and “pose/orientation refinement” modules (in reality: two distinct localisation systems). This, however, is not the topic of this work – we are purely interested in constructing a good representation of polar scans with vectors/descriptors that represent “places” well, and further pose refinement would benefit our approach equally.

The motivation for our approach as outlined above is

- 1) **Polar scans only:** We stay in the natural signal form for scanning radar and do not map to Cartesian form, in order to keep computation to a minimum, avoid interpolation artefacts, and minimise the number of settings and hyperparameters.
- 2) **Spatial frequencies in power returns:** In implementing Equation (1) we use the Fast Fourier Transform from `numpy`³. We show in Section IV that this leads to a marked improvement in localisation success than if we were to match radial power returns themselves.
- 3) **Discriminativeness:** As Equation (2) is based on residuals to cluster centres, the VLAD descriptor effectively

²e.g. if there were 1000 scans in a map, each with 400 azimuths, we perform clustering on $400 \times 1000 = 400000$ vectors

³numpy.org/doc/stable/reference/routines.fft.html

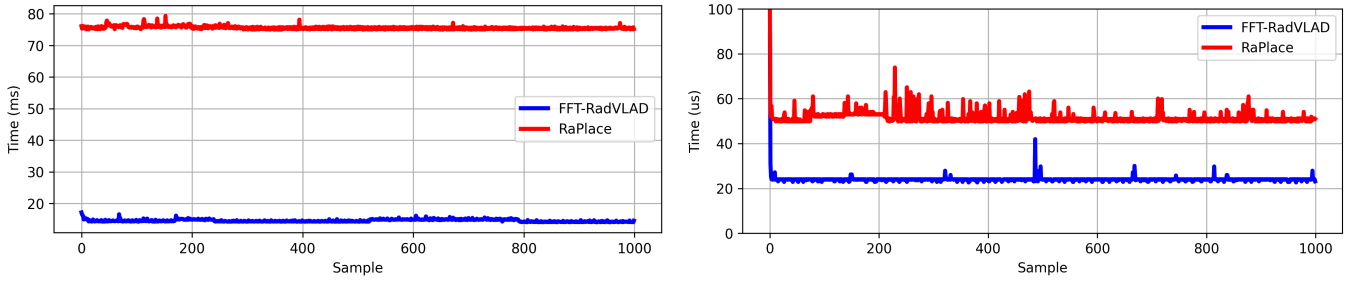


Fig. 2: *Top*: 1000 samples of time taken to **build representations** for FFT-RadVLAD, our method (blue), as compared to RaPlace from [12] (orange). *Bottom*: 1000 samples of time taken to **compute representation distance**. These samples were collected by running processes on an *Apple M2 Pro* with 12 cores and with 16 GB LPDDR5 memory.

captures information about the distribution of radial frequency responses *relative to each other* (not just their values), and this higher-order information is important for uniquely representing inputs.

- 4) **Rotation invariance**: In Equation (2), the order in which radial frequency responses at particular headings are mapped to a nearest cluster and then aggregated is irrelevant.

Note that in comparison to *RaPlace* [12], even though shifts along one radial return do not feature in the magnitude of our Fourier Transform in Equation (1)⁴, we do not have total shift invariance using a Radon and Fourier transform combination. Also, we rely on very high-dimensional descriptors (with length equal to the number of range bins \times the number of cluster centres). However, there are two important points to consider in comparing our method to [12]. Firstly, the informativeness of our longer descriptor leads to **much bigger performance benefits** (see Figure 5, with experimental verification in Sections IV and V below). Secondly, and critically, despite the length of our descriptor, our method is **much more computationally efficient** than [12] (see Figure 2 *Right*, explained further in Section V below), as our vectors are compared with simple Euclidean distances rather than circular cross-correlation which itself requires two Fourier transforms and an inverse Fourier Transform. We also build representations more quickly than [12] (Figure 2 *Left*), as we do not use polar-to-Cartesian mapping or the Radon Transform prior to the Fourier Transform.

IV. EXPERIMENTS

A. Dataset

We evaluate our method in training and testing across urban data collected in the *Oxford Radar RobotCar Dataset* [1]. The dataset was collected using an autonomous-capable *Nissan LEAF*. This follows the original *Oxford RobotCar Dataset* [19] route and over 32 traversals in different traffic, weather and lighting conditions, totalling ≈ 280 km of driving. This features a *CTS350-X Navtech* frequency-modulated continuous-wave (FMCW), scanning radar with operating frequency range

⁴For $g(r, \theta_j) = f(r + \delta r, \theta_j)$ we have $\hat{g}(\rho, \theta_j) = e^{+j\rho\delta r} \hat{f}(\rho, \theta_j)$ with some δr along a particular θ_j

76 GHz to 77 GHz and scan rate is 4 Hz. The *CTS350-X Navtech* rotates about its vertical axis while transmitting and receiving frequency-modulated radio waves. Scans have 3768 range bins at a resolution of 4.38 cm, with total range 165 m. There are 400 azimuths (resolution 0.9°).

In contrast to all prior radar place recognition work, we use *all* trajectories from this dataset, with the exception of only *-partial* completions of the central Oxford route. The 30 “experiences” used are listed in Table II. Full results are available in Table III. There are a total of $30^2 - 30 = 870$ pairs of unique experiences. For each pair, we use one experience as the *reference* trajectory or map to localise to and the other experience for *query* frames. This is the most comprehensive evaluation of place recognition over this dataset to date.

A foray typically consists of 8000 to 9000 scans. We *downsample* the framerate, taking every 10th scan. Thus, each experience features ≈ 800 to 900 places. Note that this corresponds to about $\frac{10}{4} = 2.5$ s during which time at 20 mph or 8.9408 m s^{-1} the vehicle travels about $8.9408 \times 2.5 = 22.352 \text{ m s}^{-1}$ – the typical distance between consecutive places.

B. Performance metrics

To assess the place recognition performance, we use Recall@N (R@N), which measures the percentage of query frames which have a nearest neighbour in the map which is actually close in physical space. For this we use a “difference matrix” in Figure 3 *Right* with the embedding distances (Euclidean) between live and map features. Localisation is successful if the nearest neighbour for a query embedding (rows) is a reference embedding (column) which is in truth is close to the query location in physical space. For this ground truth, in Figure 3 *Right*, we use the GPS/INS provided in the *Oxford Radar RobotCar Dataset* (a NovAtel SPAN-CPT ALIGN inertial and GPS navigation system), and consider a match to be good if it is within 25 m – a very commonly accepted threshold, e.g. as is used in [20], [21].

C. Baselines & ablation

The methods for comparison are:

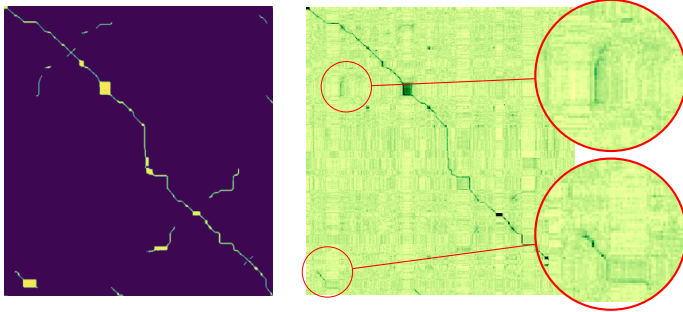


Fig. 3: *Left*: Ground truth GPS difference matrix for the $\approx 800 \times 800$ possible place correspondences between sequences 2019-01-18-15-20-12 and 2019-01-15-12-01-32. *Right*: Corresponding embedding distance matrix for FFT-RadVLAD. Red insets show revisits in the opposite lane/direction (top) and in the same lane/direction (bottom).

- ① RingKey: from [22], [2]⁵. This method consists of turning the polar array into a vector by simply finding the average of returns at distinct ranges around the vehicle – e.g. collapsing Figure 4 into a single row. Note that we do not use the additional orientation refinement from [22], as distances between row-reduced vectors and orientation scores are separate, i.e. these form a hierarchy of localisers as mentioned in Section III and we are interested in comparing the engineering of vector representations.
- ② RaPlace: from [14]⁶ as described in Section III. Through maximising circular cross-correlation, this method actually does recover orientation. However, in contrast to ②, this orientation score is what is used for place recognition/similarity measurement.
- ③ RadVLAD: from Section III. This involves VLAD descriptors but *no Fourier Transform* (i.e. we cluster, etc the raw radar signals).
- ④ FFT-RadVLAD: from Section III. This is as per ③ but in this case we use the radial frequency responses rather than raw radar signals.

Here, ① and ② are competitors, while ③ and ④ serve as an ablation study for the two critical components of our work.

Note that the evaluation of RaPlace in [12] on the *Oxford Radar RobotCar Dataset* was restricted to experiences from 2019-01-16 and 2019-01-18, while our evaluation covers the entire month of data. Also in contrast to [12], we do not look for loop closures *within an experience* – which may be scarce – instead focusing on the inter-experience setup, where loop closures are abundant (every frame in the query sequence has matches in the reference sequence).

⁵Open implementation at github.com/irapkaist/scancontext/tree/master/fast_evaluator_radar

⁶Open implementation at github.com/hyesu-jang/RaPlace/blob/main/PYTHON/RaPlace.py

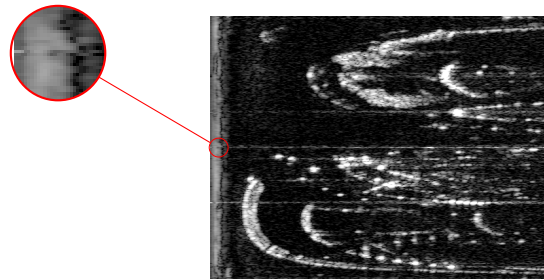


Fig. 4: *Example polar scan*, with maximum range limited to 1024 pixels and then resized to 400×512 . The zoomed in inset (red) shows **returns from near the vehicle** (first few range columns).

D. Settings & hyperparameters

The polar scans are originally 400×3768 . For the methods based on polar scans (RingKey, RadVLAD, FFT-RadVLAD) we suppress the first 60 range bins by setting them to zero. This is motivated in Figure 4, where the early returns are likely dominated by the ego-vehicle itself and/or ground returns. In practice, we found that this boosted performance for all methods. For quicker processing, we then rescale the 400×3768 polar to 400×512 – scaling only range.

1) *First baseline (RingKey)*: For RingKey we reduce the 400×512 polar scan to a 1×512 vector by average-pooling the azimuth dimension. This is a longer representation than is used in [2], but we will show in Section V-C that there are no settings for RingKey which allows it to approach the performance of RadVLAD or FFT-RadVLAD.

2) *Second baseline (RaPlace)*: Here, a Cartesian scan is made 256 pixels square, and we use a Cartesian pixel resolution of 1.2717 m. This means – with the vehicle in the centre of the Cartesian projection – that the range is $\frac{256}{2} \times 1.2717 = 162.7776$ m. With a radar range resolution of 4.32 cm (see Section IV-A) for the polar variants above range is given by $3768 \times 0.0432 = 162.7776$ m. Thus, *all methods are presented with precisely the same range-bearing information out to the same range*. In [12], after the Radon transform, the Sinograms are scaled to 10% of their size. We use 25% by default, but explore the effect of this and the Cartesian image size in Section V-C (where, again, there are no settings which allow RaPlace to approach RadVLAD or FFT-RadVLAD).

3) *First ablation (RadVLAD)*: VLAD descriptors are computed with 64 cluster centres. Cluster centres themselves are computed from each reference trajectory. For this we use kmeans++ [23] with tolerance 1×10^{-4} and running only a single centroid seed.

4) *Second ablation (FFT-RadVLAD)*: With discrete radial returns in the form 1×512 we perform the 512-point FFT, resulting in frequency response maps of the same shape as the input polar array (400×512).

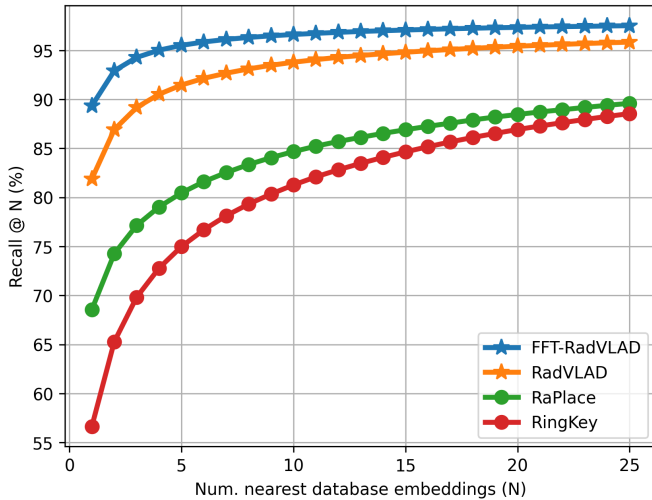


Fig. 5: Recall@1-50 curves for variants of our method (RadVLAD and FFT-RadVLAD) and two competitors (RingKey and RaPlace). As a guide to reading this result: for $N = 20$ consider that *Ring Key* has approximately 85% Recall@20 – this means that, 85% of the time, when a query has 20 candidate nearest neighbours returned, at least 1 of them is in fact a nearby place. Of course, for $N \rightarrow \infty$ we will eventually return the entire map where we are guaranteed to find a match (Recall@ $\infty \rightarrow 100\%$). For all N , our FFT-RadVLAD performs best.

V. RESULTS

Experimental results are presented in Figure 5 and Tables I and II and are discussed below. Full results are available in Table III.

A. Establishing an exhaustive open baseline for the Oxford Radar RobotCar Dataset

Table II shows the Recall@1 as an aggregate for each experience as a query over all possible maps. Full results are available in Table III. The entries in Table II are read as RingKey / RaPlace / RadVLAD / FFT-RadVLAD or ① / ② / ③ / ④ as defined in Section IV-C with RadVLAD and FFT-RadVLAD or ③ or ④ being the third and fourth entries in each cell, corresponding to variants of our proposed system. To complement this, Figure 5 shows the summarised Recall@1-50 plots which are averaged (mean) over all of the experience pairs from Table II. For every one of the 870 query-reference trajectory pairs that are aggregated in Table II, FFT-RadVLAD is the top-performer. This is reaffirmed in Figure 5 which is averaged over all 870 experiments for the full range of N .

B. Measuring computational efficiency

Importantly, our FFT-RadVLAD is more computationally efficient than RaPlace. This is shown in Figure 2 where time taken to build representations (RaPlace representation building includes a polar to Cartesian conversion) is reduced

Azis [px]	Bins [px]	Length [px]	Recall@1 [%]
50	1884	128	48.31
100	1884	128	49.44
200	1884	128	49.77
400	1884	128	50.23
50	3768	128	51.81
100	3768	128	52.26
200	3768	128	52.37
400	3768	128	52.93
50	1884	512	47.86
100	1884	512	48.53
200	1884	512	48.87
400	1884	512	50.23
50	3768	512	51.58
100	3768	512	52.26
200	3768	512	52.14
400	3768	512	52.60

Scale [%]	Res. [m]	Width [px]	Recall@1 [%]
10	1.2717	256	58.92
10	0.63585	512	61.96
10	2.5424	128	49.89
10	0.3178	1024	64.56
20	1.2717	256	62.98
20	0.63585	512	64.90
20	2.5424	128	58.35
20	0.3178	1024	65.69
30	1.2717	256	64.56
30	0.63585	512	66.25
30	2.5424	128	61.63
30	0.3178	1024	66.59
40	1.2717	256	65.24
40	0.63585	512	67.16
40	2.5424	128	63.54
40	0.3178	1024	66.93

TABLE I: Recall@1 (%) for variations of *Top*: RingKey. *Bottom*: RaPlace with best-case indicated red. To explore these combinations of settings we use as localisation and map experiences only 2019-01-10-11-46-21 and 2019-01-11-13-24-51.

by $\approx 75\%$ and time taken to compute distances between representations by $\approx 50\%$.

C. Best-case baselines

Table I *Left* shows an exhaustive variation of three parameters for RingKey. They are: the maximum radar range (**Bins [px]**), the number of discrete headings in the polar scan before vector reduction/azimuth pooling (**Azis [px]**), and the number of discrete range bins in the reduced vector representation (**Length [px]**). We are not able to exceed the performance in Table II sufficiently to approach the performance of RadVLAD or FFT-RadVLAD.

Table I *Right* similarly shows exhaustive variation of three parameters for RaPlace. They are: the real-world size of a Cartesian pixel (**Res. [m]**), the number of pixels to a side for the Cartesian scan (**Width [px]**), and the downscaling factor applied (**Scale [%]**) prior to applying the Radon transform. We are similarly not able to exceed the performance of Table II sufficiently to approach RadVLAD or FFT-RadVLAD.

VI. CONCLUSION

We have presented an open implementation of a simple method for extremely robust radar place recognition. The learned components of our system (cluster centres) are found in an unsupervised fashion without labels and with only a single hyperparameter (number of cluster centres), meaning that RadVLAD or FFT-RadVLAD can be extremely easily

	mean (2019-01-*)	median (2019-01-*)
2019-01-10-11-46-21	56.2 / 68.2 / 81.4 / 89.0	57.2 / 69.2 / 83.5 / 91.2
2019-01-11-13-24-51	55.5 / 64.5 / 80.9 / 87.0	56.6 / 65.5 / 81.9 / 88.1
2019-01-14-14-48-55	63.7 / 74.1 / 86.7 / 93.6	63.9 / 74.3 / 88.0 / 94.7
2019-01-16-13-09-37	58.2 / 67.8 / 83.7 / 91.9	59.1 / 69.4 / 85.4 / 93.1
2019-01-18-12-42-34	60.5 / 69.5 / 85.8 / 92.0	60.6 / 71.4 / 87.8 / 91.6
2019-01-10-12-32-52	58.1 / 69.7 / 84.8 / 91.7	60.0 / 69.6 / 85.6 / 93.0
2019-01-11-14-02-26	61.8 / 73.8 / 86.3 / 92.7	62.8 / 74.4 / 87.5 / 94.1
2019-01-15-12-01-32	49.2 / 57.5 / 66.5 / 71.5	48.7 / 57.4 / 66.7 / 72.4
2019-01-16-13-42-28	46.6 / 63.5 / 75.4 / 85.3	47.7 / 64.1 / 76.0 / 85.8
2019-01-18-14-14-42	60.2 / 74.5 / 87.8 / 92.5	61.1 / 75.1 / 88.4 / 93.2
2019-01-10-14-02-34	63.7 / 74.6 / 87.4 / 93.0	65.4 / 74.3 / 87.5 / 94.0
2019-01-11-14-37-14	59.8 / 71.0 / 82.5 / 89.4	58.2 / 71.2 / 82.9 / 90.1
2019-01-16-14-15-33	45.6 / 61.4 / 74.9 / 85.1	46.7 / 61.7 / 75.7 / 86.0
2019-01-18-14-46-59	59.5 / 74.3 / 86.4 / 92.5	59.8 / 74.8 / 87.3 / 93.1
2019-01-14-12-05-52	57.6 / 69.6 / 84.3 / 91.2	56.9 / 70.5 / 85.5 / 92.2
2019-01-15-13-06-37	59.5 / 69.2 / 85.6 / 91.7	60.7 / 70.6 / 87.6 / 92.8
2019-01-17-11-46-31	59.8 / 71.0 / 87.1 / 94.0	60.6 / 71.1 / 88.4 / 94.5
2019-01-18-15-20-12	61.2 / 73.0 / 86.6 / 92.5	61.5 / 74.0 / 87.2 / 93.1
2019-01-10-14-50-05	59.6 / 72.2 / 83.7 / 90.7	60.0 / 72.8 / 83.3 / 91.8
2019-01-14-12-41-28	60.1 / 69.5 / 84.6 / 93.0	61.2 / 70.8 / 85.6 / 94.6
2019-01-15-13-53-14	61.9 / 73.2 / 85.1 / 91.7	62.9 / 75.5 / 86.5 / 92.5
2019-01-17-12-48-25	56.1 / 68.5 / 84.8 / 92.7	56.2 / 69.4 / 86.1 / 93.7
2019-01-10-15-19-41	60.4 / 71.4 / 87.6 / 93.8	60.8 / 74.8 / 88.3 / 94.2
2019-01-14-13-38-21	55.8 / 68.6 / 86.1 / 92.7	56.1 / 67.7 / 86.7 / 94.0
2019-01-15-14-24-38	60.9 / 72.7 / 85.4 / 92.3	61.8 / 74.0 / 86.1 / 93.4
2019-01-17-13-26-39	62.0 / 73.9 / 85.4 / 92.4	62.8 / 74.1 / 86.9 / 93.1
2019-01-11-12-26-55	62.2 / 73.5 / 87.3 / 93.0	62.7 / 73.1 / 88.6 / 94.0
2019-01-14-14-15-12	61.8 / 71.7 / 84.0 / 90.7	64.9 / 73.1 / 86.7 / 93.1
2019-01-16-11-53-11	57.8 / 68.2 / 80.8 / 88.6	58.6 / 69.4 / 80.7 / 88.3
2019-01-17-14-03-00	58.8 / 69.2 / 85.6 / 94.2	58.6 / 67.1 / 87.0 / 95.3

TABLE II: Each entry shows the Recall@1 localisation performance (as a percentage, %) for methods ①/②/③/④ as described in Section IV-C. Each row corresponds to a trajectory (grey) used as the query experience, and the mean and median columns are then aggregates of this query experience over each of every other trajectory as the reference sequence. There are 30 experiences in total, and so each column represents 29 localisation experiments, and over 30 rows we therefore have $29 \times 30 = 870$ localisation experiments. The **mean over all queries** for RingKey / RaPlace / RadVLAD / FFT-RadVLAD is 56.64 / 68.56 / 81.88 / **89.35** and the medians are 57.67 / 69.55 / 83.74 / **91.52**. As can be seen, FFT-RadVLAD (Ours) results in the best performance (**bold**), in every single case.

and quickly included in existing radar localisation pipelines. Our system was demonstrated over the most exhaustive *Oxford Radar RobotCar Dataset* evaluation to date, and outperforms two other open-sourced competitors. We trust that the open-sourcing of this system and the full list of results will prompt more research into this problem.

In the future, we will extend the system to other classes of radar, e.g. as in *nusenes* [24] as investigated for place recognition in [25].

ACKNOWLEDGEMENTS

This work was supported by EPSRC Programme Grant “From Sensing to Collaboration” (EP/V000748/1). We are also grateful to our partners at Navtech Radar.

REFERENCES

- [1] D. Barnes, M. Gadd, P. Murcutt, P. Newman, and I. Posner, “The oxford radar robotcar dataset: A radar extension to the oxford robotcar dataset,” in *International Conference on Robotics and Automation (ICRA)*, 2020.
- [2] G. Kim, Y. S. Park, Y. Cho, J. Jeong, and A. Kim, “Mulran: Multimodal range dataset for urban place recognition,” in *International Conference on Robotics and Automation (ICRA)*, 2020.
- [3] M. Sheeny, E. De Pellegrin, S. Mukherjee, A. Ahrabian, S. Wang, and A. Wallace, “Radiate: A radar dataset for automotive perception in bad weather,” in *2021 IEEE International Conference on Robotics and Automation (ICRA)*. IEEE, 2021, pp. 1–7.
- [4] Ş. Săftescu, M. Gadd, D. De Martini, D. Barnes, and P. Newman, “Kidnapped radar: Topological radar localisation using rotationally-invariant metric learning,” in *2020 International Conference on Robotics and Automation (ICRA)*. IEEE, 2020, pp. 4358–4364.

- [5] D. Barnes and I. Posner, “Under the radar: Learning to predict robust keypoints for odometry estimation and metric localisation in radar,” in *2020 International Conference on Robotics and Automation (ICRA)*. IEEE, 2020, pp. 9484–9490.
- [6] M. Gadd, D. De Martini, and P. Newman, “Look around you: Sequence-based radar place recognition with learned rotational invariance,” in *2020 IEEE/ION Position, Location and Navigation Symposium (PLANS)*. IEEE, 2020, pp. 270–276.
- [7] W. Wang, P. P. de Gusmo, B. Yang, A. Markham, and N. Trigoni, “RadarLoc: Learning to Relocalize in FMCW Radar,” in *International Conference on Robotics and Automation (ICRA)*, 2021.
- [8] J. Komorowski, M. Wysoczanska, and T. Trzcinski, “Large-scale topological radar localization using learned descriptors,” in *Neural Information Processing: 28th International Conference, ICONIP 2021, Sanur, Bali, Indonesia, December 8–12, 2021, Proceedings, Part II 28*. Springer, 2021, pp. 451–462.
- [9] M. Gadd, D. De Martini, and P. Newman, “Contrastive learning for unsupervised radar place recognition,” in *2021 20th International Conference on Advanced Robotics (ICAR)*. IEEE, 2021, pp. 344–349.
- [10] Z. Hong, Y. Petillot, A. Wallace, and S. Wang, “Radarslam: A robust simultaneous localization and mapping system for all weather conditions,” *The International Journal of Robotics Research*, vol. 41, no. 5, pp. 519–542, 2022.
- [11] D. Adolfsson, M. Karlsson, V. Kubelka, M. Magnusson, and H. Andreasson, “Tbv radar slam: trust but verify loop candidates,” *arXiv preprint arXiv:2301.04397*, 2023.
- [12] H. Jang, M. Jung, and A. Kim, “RaPlace: Place Recognition for Imaging Radar using Radon Transform and Mutable Threshold,” in *IEEE/RSJ International Conference on Intelligent Robots and Systems (IROS)*, 2023.
- [13] J. Yuan, P. Newman, and M. Gadd, “Off the Radar: Variational Uncertainty-Aware Unsupervised Radar Place Recognition for Introspective Querying and Map Maintenance,” in *IEEE/RSJ International Conference on Intelligent Robots and Systems (IROS)*, 2023.
- [14] S. Lu, X. Xu, H. Yin, Z. Chen, R. Xiong, and Y. Wang, “One ring to rule them all: Radon sinogram for place recognition, orientation and translation estimation,” in *2022 IEEE/RSJ International Conference on Intelligent Robots and Systems (IROS)*. IEEE, 2022, pp. 2778–2785.
- [15] G. Beylkin, “Discrete radon transform,” *IEEE transactions on acoustics, speech, and signal processing*, vol. 35, no. 2, pp. 162–172, 1987.
- [16] R. Weston, M. Gadd, D. De Martini, P. Newman, and I. Posner, “Fastmby: Leveraging translational invariance of the fourier transform for efficient and accurate radar odometry,” in *International Conference on Robotics and Automation (ICRA)*.
- [17] Y. S. Park, Y.-S. Shin, and A. Kim, “Pharao: Direct radar odometry using phase correlation,” in *International Conference on Robotics and Automation (ICRA)*.
- [18] R. Arandjelovic and A. Zisserman, “All about vlad,” in *Proceedings of the Conference on Computer Vision and Pattern Recognition*, 2013, pp. 1578–1585.
- [19] W. Maddern, G. Pascoe, C. Linegar, and P. Newman, “1 year, 1000 km: The oxford robotcar dataset,” *The International Journal of Robotics Research*, 2017.
- [20] R. Arandjelovic, P. Gronat, A. Torii, T. Pajdla, and J. Sivic, “Netvlad: Cnn architecture for weakly supervised place recognition,” in *Conference on Computer Vision and Pattern Recognition*, 2016.
- [21] G. Berton, C. Masone, and B. Caputo, “Rethinking visual geolocalization for large-scale applications,” in *IEEE/CVF Conference on Computer Vision and Pattern Recognition*, 2022.
- [22] G. Kim and A. Kim, “Scan context: Egocentric spatial descriptor for place recognition within 3d point cloud map,” in *IEEE/RSJ International Conference on Intelligent Robots and Systems (IROS)*, 2018.
- [23] D. Arthur and S. Vassilvitskii, “K-means++ the advantages of careful seeding,” in *Proceedings of the eighteenth annual ACM-SIAM symposium on Discrete algorithms*, 2007, pp. 1027–1035.
- [24] H. Caesar, V. Bankiti, A. H. Lang, S. Vora, V. E. Liong, Q. Xu, A. Krishnan, Y. Pan, G. Baldan, and O. Beijbom, “nusenes: A multimodal dataset for autonomous driving,” in *Proceedings of the IEEE/CVF conference on computer vision and pattern recognition*, 2020, pp. 11 621–11 631.
- [25] K. Cai, B. Wang, and C. X. Lu, “Autoplace: Robust place recognition with single-chip automotive radar,” in *2022 International Conference on Robotics and Automation (ICRA)*. IEEE, 2022, pp. 2222–2228.

	2019-01-11-14-26-21	2019-01-11-13-24-51	2019-01-13-14-48-35	2019-01-16-19-33-37	2019-01-18-22-45-34	2019-01-19-23-32-52	2019-01-11-14-02-26	2019-01-15-12-01-32
2019-01-10-11-46-21	- / - / -	52.6 / 63.9 / 87.0 / 93.1	54.1 / 71.4 / 83.1 / 83.9	59.1 / 67.5 / 85.9 / 94.2	56.2 / 71.1 / 84.4 / 90.6	73.6 / 77.1 / 92.0 / 96.7	57.0 / 67.6 / 87.2 / 94.2	45.6 / 53.3 / 62.3 / 71.9
2019-01-11-13-24-51	54.3 / 63.0 / 82.1 / 88.8	57.3 / 62.5 / 86.1 / 92.5	57.1 / 65.3 / 77.8 / 83.9	59.7 / 67.5 / 81.6 / 87.4	58.6 / 67.3 / 80.5 / 87.5	60.2 / 64.8 / 84.1 / 91.2	58.2 / 69.5 / 82.1 / 89.9	41.4 / 49.8 / 58.6 / 68.2
2019-01-14-14-48-55	63.0 / 74.9 / 86.7 / 94.2	61.3 / 69.8 / 84.3 / 93.2	- / - / -	63.0 / 74.4 / 89.3 / 94.9	60.4 / 74.2 / 83.6 / 92.8	69.2 / 76.6 / 89.4 / 93.7	62.1 / 76.5 / 86.6 / 91.8	48.5 / 56.6 / 66.0 / 70.1
2019-01-16-13-09-37	55.2 / 68.7 / 84.3 / 92.7	59.7 / 65.0 / 82.2 / 90.9	57.9 / 69.6 / 84.6 / 93.2	- / - / -	57.7 / 66.2 / 82.3 / 92.9	54.9 / 68.8 / 82.7 / 92.1	52.9 / 70.3 / 85.4 / 92.7	41.6 / 54.7 / 62.7 / 70.7
2019-01-18-12-34-24	55.7 / 69.6 / 84.9 / 94.3	55.1 / 59.3 / 85.8 / 90.6	52.9 / 64.5 / 81.0 / 85.3	65.9 / 70.2 / 87.2 / 93.0	65.9 / 70.2 / 87.2 / 93.0	61.9 / 75.0 / 91.6 / 95.6	56.7 / 71.9 / 86.8 / 93.8	52.0 / 58.5 / 69.8 / 73.1
2019-01-10-12-32-52	63.0 / 76.1 / 87.7 / 94.1	63.7 / 62.5 / 86.1 / 92.5	57.1 / 71.5 / 81.4 / 83.0	56.7 / 71.2 / 84.8 / 90.2	58.6 / 71.2 / 84.8 / 90.2	63.9 / 69.3 / 88.4 / 92.9	60.0 / 70.4 / 82.2 / 92.2	46.8 / 56.7 / 64.2 / 69.9
2019-01-11-14-26-21	49.4 / 57.0 / 64.4 / 72.0	44.0 / 50.2 / 62.3 / 70.1	50.3 / 58.3 / 68.1 / 73.1	47.7 / 60.1 / 65.4 / 70.6	50.6 / 59.0 / 68.3 / 71.7	46.1 / 60.8 / 66.0 / 72.7	49.5 / 60.5 / 67.8 / 73.7	49.0 / 60.0 / 70.0 / 74.7
2019-01-16-13-09-37	49.1 / 56.7 / 70.0 / 86.2	42.7 / 56.7 / 73.7 / 83.7	42.3 / 60.6 / 73.1 / 81.8	42.3 / 60.6 / 73.1 / 81.8	42.3 / 60.6 / 73.1 / 81.8	49.6 / 63.0 / 77.6 / 85.3	48.1 / 59.5 / 75.4 / 81.9	36.6 / 52.9 / 60.9 / 67.2
2019-01-18-14-14-42	58.8 / 74.6 / 80.0 / 93.4	58.8 / 70.2 / 85.4 / 92.8	56.8 / 73.9 / 84.9 / 93.9	62.8 / 75.8 / 90.1 / 94.9	61.7 / 74.2 / 88.4 / 96.1	60.2 / 72.3 / 89.7 / 94.2	61.1 / 72.4 / 88.5 / 92.7	50.8 / 61.2 / 71.8 / 75.7
2019-01-10-14-02-34	62.9 / 76.2 / 86.1 / 94.1	55.0 / 70.5 / 85.5 / 94.8	59.1 / 79.3 / 86.3 / 94.9	60.7 / 70.1 / 86.8 / 90.8	64.7 / 73.1 / 88.6 / 93.3	67.6 / 74.1 / 88.1 / 95.2	61.4 / 75.3 / 87.9 / 93.9	47.3 / 53.0 / 70.1 / 73.9
2019-01-11-14-37-14	55.6 / 72.4 / 83.1 / 90.5	63.2 / 69.7 / 80.3 / 89.3	56.0 / 73.6 / 84.4 / 89.2	58.8 / 69.7 / 84.1 / 89.2	60.8 / 71.2 / 82.0 / 90.5	59.7 / 72.8 / 81.9 / 90.1	63.1 / 75.3 / 84.8 / 93.7	46.0 / 56.4 / 62.9 / 66.7
2019-01-16-13-09-37	40.0 / 49.2 / 73.4 / 84.4	40.0 / 55.2 / 72.3 / 84.7	40.8 / 53.4 / 67.7 / 80.5	46.2 / 63.4 / 87.9 / 91.7	42.9 / 51.6 / 78.8 / 89.0	44.9 / 61.5 / 79.5 / 88.5	41.4 / 54.0 / 71.4 / 82.6	34.2 / 36.7 / 56.4 / 67.1
2019-01-18-14-48-55	56.7 / 75.7 / 83.6 / 94.0	60.7 / 70.9 / 87.3 / 94.1	62.5 / 74.7 / 88.5 / 94.8	57.4 / 76.0 / 87.3 / 92.4	57.4 / 76.0 / 87.3 / 92.4	64.9 / 72.2 / 88.9 / 95.2	55.2 / 77.0 / 87.6 / 92.8	50.1 / 61.2 / 71.4 / 75.8
2019-01-14-12-05-32	57.1 / 69.2 / 82.7 / 92.9	61.0 / 68.4 / 84.3 / 92.1	56.5 / 70.9 / 83.4 / 93.4	57.7 / 72.5 / 81.8 / 90.5	54.2 / 66.9 / 80.3 / 92.5	57.7 / 67.3 / 85.6 / 94.3	59.0 / 71.8 / 83.5 / 92.1	48.2 / 59.2 / 65.8 / 73.5
2019-01-15-13-06-37	64.7 / 68.2 / 86.8 / 93.1	59.4 / 63.3 / 85.7 / 92.9	60.3 / 69.3 / 87.4 / 93.8	63.3 / 65.8 / 86.8 / 93.3	64.2 / 69.7 / 85.0 / 92.6	63.7 / 66.5 / 88.8 / 92.5	57.5 / 71.9 / 84.3 / 94.2	53.4 / 59.1 / 72.1 / 77.4
2019-01-11-14-37-14	57.4 / 69.7 / 86.5 / 91.8	66.1 / 68.3 / 87.8 / 94.2	57.6 / 73.1 / 86.8 / 94.7	62.0 / 69.3 / 89.3 / 94.0	55.2 / 67.9 / 88.6 / 94.4	60.0 / 71.8 / 89.3 / 94.4	54.3 / 71.0 / 85.0 / 94.2	42.4 / 54.4 / 69.2 / 74.0
2019-01-18-15-20-12	56.4 / 70.0 / 85.9 / 93.7	54.2 / 64.5 / 81.0 / 91.8	63.2 / 77.4 / 86.6 / 93.5	57.7 / 68.2 / 85.9 / 91.4	59.8 / 66.8 / 87.4 / 93.2	49.3 / 72.0 / 80.2 / 89.5	54.3 / 71.0 / 85.0 / 94.2	47.3 / 53.0 / 71.3 / 74.0
2019-01-10-14-02-34	61.7 / 72.9 / 86.7 / 92.8	61.7 / 68.4 / 84.9 / 91.6	58.3 / 73.9 / 83.5 / 91.2	62.9 / 69.7 / 84.2 / 92.2	65.1 / 73.2 / 82.9 / 89.3	62.2 / 74.9 / 87.5 / 91.7	61.4 / 74.9 / 83.9 / 90.7	46.6 / 56.2 / 63.2 / 69.4
2019-01-14-12-41-24	59.9 / 68.8 / 87.5 / 94.9	57.8 / 63.5 / 83.9 / 92.9	60.3 / 74.2 / 87.6 / 94.7	60.6 / 69.0 / 82.1 / 93.8	60.5 / 70.2 / 82.2 / 93.5	62.3 / 74.0 / 85.2 / 94.7	58.9 / 69.4 / 83.4 / 92.6	49.5 / 55.6 / 64.8 / 73.8
2019-01-15-13-53-14	60.1 / 71.2 / 86.0 / 92.8	61.4 / 69.2 / 86.8 / 93.5	61.4 / 74.5 / 85.2 / 92.6	61.0 / 70.7 / 85.9 / 94.6	63.5 / 72.1 / 84.9 / 92.5	63.8 / 75.2 / 86.4 / 93.6	60.6 / 72.1 / 85.9 / 93.6	50.9 / 56.6 / 69.1 / 74.2
2019-01-17-12-28-48	58.7 / 66.9 / 86.3 / 95.2	56.0 / 66.7 / 82.9 / 92.4	54.3 / 69.9 / 81.2 / 92.8	58.2 / 70.8 / 88.5 / 95.1	56.1 / 67.8 / 85.4 / 93.1	60.1 / 72.3 / 89.3 / 94.7	57.1 / 66.8 / 83.0 / 92.5	45.0 / 55.0 / 64.4 / 70.5
2019-01-10-15-19-41	64.0 / 71.1 / 84.5 / 93.9	54.6 / 57.7 / 87.9 / 95.0	60.4 / 71.7 / 83.3 / 93.4	64.4 / 76.3 / 87.8 / 93.9	59.3 / 74.6 / 87.2 / 93.0	67.5 / 75.0 / 89.0 / 94.3	57.3 / 74.0 / 87.3 / 94.2	51.5 / 53.5 / 70.9 / 76.6
2019-01-13-13-26-38	54.0 / 62.1 / 81.6 / 92.7	55.0 / 58.8 / 81.3 / 93.2	55.2 / 64.0 / 85.9 / 93.2	51.2 / 73.0 / 84.9 / 92.7	54.1 / 64.0 / 81.6 / 88.5	61.3 / 63.3 / 74.1 / 81.8	53.1 / 63.3 / 74.1 / 81.8	49.4 / 54.5 / 65.5 / 70.4
2019-01-15-14-24-38	58.8 / 72.7 / 83.5 / 94.5	58.9 / 69.7 / 81.8 / 93.1	62.4 / 76.5 / 86.5 / 94.8	61.9 / 74.0 / 84.6 / 93.6	61.1 / 72.4 / 85.6 / 91.5	65.2 / 75.4 / 87.9 / 94.7	64.6 / 77.7 / 85.0 / 91.4	49.4 / 67.7 / 68.3 / 72.6
2019-01-17-13-26-38	60.7 / 76.9 / 83.0 / 91.7	58.7 / 66.0 / 80.8 / 91.4	58.5 / 71.7 / 83.5 / 93.2	62.6 / 72.7 / 88.6 / 94.6	64.0 / 74.1 / 87.3 / 91.7	61.5 / 74.9 / 86.2 / 95.1	61.0 / 75.6 / 87.1 / 94.1	46.6 / 59.4 / 69.3 / 75.3
2019-01-11-12-26-55	63.3 / 75.6 / 88.0 / 93.3	62.5 / 66.4 / 87.8 / 94.2	61.8 / 76.5 / 88.1 / 92.3	63.3 / 75.0 / 84.6 / 94.0	64.3 / 70.0 / 84.6 / 94.0	66.0 / 75.4 / 89.5 / 95.2	64.0 / 78.0 / 88.6 / 94.4	43.9 / 57.4 / 66.5 / 72.2
2019-01-14-14-15-34	60.9 / 73.7 / 83.1 / 91.1	59.2 / 67.7 / 82.5 / 91.1	63.8 / 76.6 / 87.6 / 92.9	64.7 / 75.8 / 88.8 / 93.8	63.3 / 70.8 / 83.9 / 92.8	61.4 / 72.6 / 83.8 / 93.2	59.3 / 75.3 / 83.5 / 93.3	51.1 / 54.2 / 65.4 / 71.4
2019-01-16-11-53-11	58.0 / 69.4 / 80.3 / 88.2	56.6 / 64.6 / 82.4 / 86.9	58.3 / 70.0 / 76.9 / 88.2	55.2 / 68.9 / 82.6 / 88.2	52.0 / 70.2 / 81.1 / 86.2	58.8 / 69.4 / 82.3 / 88.9	52.8 / 68.0 / 80.4 / 86.9	48.8 / 57.8 / 72.1 / 75.3
2019-01-17-14-03-00	45.4 / 63.0 / 77.6 / 85.0	50.4 / 66.9 / 83.1 / 91.2	49.6 / 64.9 / 80.7 / 87.6	47.0 / 64.1 / 81.9 / 91.7	47.0 / 64.1 / 81.9 / 91.7	53.7 / 64.1 / 82.9 / 88.5	45.4 / 63.0 / 77.6 / 85.0	38.9 / 46.1 / 57.1 / 64.9
2019-01-16-13-49-28	49.0 / 62.4 / 73.5 / 85.3	55.9 / 66.9 / 84.3 / 91.6	57.9 / 68.6 / 86.1 / 92.8	51.6 / 68.7 / 86.5 / 91.3	44.1 / 63.0 / 71.6 / 80.9	58.8 / 67.3 / 83.3 / 91.4	50.7 / 64.7 / 83.6 / 90.6	54.4 / 65.8 / 80.6 / 88.0
2019-01-11-13-24-51	46.5 / 57.8 / 69.8 / 82.7	53.8 / 64.5 / 80.2 / 86.7	53.8 / 62.7 / 78.9 / 86.9	59.5 / 65.0 / 79.9 / 86.7	55.5 / 60.6 / 79.9 / 86.7	51.7 / 62.4 / 74.5 / 84.2	54.5 / 63.0 / 76.9 / 83.4	44.5 / 52.6 / 62.9 / 69.4
2019-01-14-14-48-55	50.5 / 65.9 / 74.6 / 82.2	60.9 / 75.7 / 85.8 / 91.8	55.8 / 74.9 / 85.3 / 91.5	64.1 / 74.4 / 85.9 / 93.9	49.5 / 66.1 / 67.1 / 77.5	63.2 / 69.9 / 85.4 / 92.7	62.7 / 67.0 / 82.4 / 91.0	58.7 / 72.3 / 84.5 / 90.4
2019-01-15-13-09-37	53.7 / 66.0 / 76.4 / 88.3	50.0 / 66.6 / 86.0 / 91.5	55.7 / 65.5 / 83.4 / 92.7	53.8 / 67.1 / 82.3 / 90.4	49.5 / 67.9 / 70.4 / 83.6	61.3 / 63.5 / 78.0 / 90.0	52.9 / 66.0 / 81.6 / 87.5	59.1 / 65.2 / 80.8 / 86.7
2019-01-17-13-26-38	62.3 / 76.9 / 86.1 / 94.9	62.3 / 69.1 / 81.6 / 90.6	59.0 / 70.3 / 83.8 / 91.7	54.0 / 63.4 / 84.0 / 90.6	54.0 / 63.4 / 84.0 / 90.6	54.0 / 63.4 / 84.0 / 90.6	54.0 / 63.4 / 84.0 / 90.6	54.0 / 63.4 / 84.0 / 90.6
2019-01-10-12-32-52	46.7 / 61.9 / 70.5 / 82.9	57.0 / 71.0 / 82.8 / 89.3	63.4 / 67.8 / 85.0 / 91.2	59.7 / 67.7 / 82.5 / 90.5	48.8 / 60.6 / 68.4 / 82.2	59.8 / 66.4 / 83.3 / 89.3	55.7 / 66.0 / 81.1 / 87.3	53.3 / 65.6 / 78.0 / 85.8
2019-01-11-14-02-34	46.1 / 64.2 / 73.8 / 85.4	57.5 / 75.0 / 86.6 / 92.7	57.0 / 72.2 / 84.6 / 92.7	62.2 / 77.5 / 88.8 / 93.5	45.3 / 62.5 / 67.5 / 82.0	58.3 / 69.5 / 85.5 / 91.3	57.0 / 73.0 / 82.0 / 90.1	52.5 / 65.8 / 79.0 / 88.4
2019-01-15-12-01-32	47.7 / 56.4 / 61.5 / 66.6	51.1 / 56.5 / 64.8 / 71.5	49.7 / 56.0 / 65.4 / 70.5	49.7 / 56.0 / 65.4 / 70.5	49.7 / 56.0 / 65.4 / 70.5	46.8 / 56.2 / 65.6 / 73.2	46.1 / 58.6 / 66.3 / 71.5	52.1 / 60.1 / 67.9 / 72.3
2019-01-16-13-49-28	54.5 / 65.1 / 78.6 / 88.8	45.3 / 63.3 / 76.9 / 84.0	42.3 / 61.1 / 68.4 / 81.4	43.6 / 62.7 / 75.0 / 85.7	51.1 / 79.7 / 74.4 / 89.3	45.9 / 59.2 / 74.6 / 82.5	44.1 / 56.2 / 74.0 / 81.1	49.3 / 59.0 / 71.7 / 79.6
2019-01-10-14-24-38	54.5 / 68.6 / 75.3 / 86.0	62.7 / 68.9 / 87.5 / 92.1	61.1 / 68.1 / 87.2 / 93.1	64.7 / 72.7 / 85.9 / 91.4	54.1 / 69.3 / 82.7 / 90.9	69.6 / 76.5 / 87.1 / 92.8	61.4 / 68.0 / 80.1 / 89.5	59.1 / 67.1 / 81.8 / 90.7
2019-01-11-14-37-14	48.0 / 62.9 / 72.3 / 81.1	62.5 / 71.5 / 81.3 / 88.8	55.7 / 65.9 / 79.9 / 86.5	- / - / -	- / - / -	61.5 / 74.3 / 85.5 / 89.2	61.5 / 74.3 / 85.5 / 89.2	65.6 / 69.9 / 90.9 / 90.9
2019-01-16-14-15-34	54.0 / 79.3 / 75.3 / 93.9	42.9 / 55.8 / 69.1 / 82.6	42.9 / 57.9 / 72.6 / 84.7	42.7 / 63.4 / 75.7 / 83.5	- / - / -	45.5 / 53.6 / 68.9 / 78.0	41.5 / 56.0 / 71.7 / 82.4	44.1 / 54.2 / 68.2 / 79.6
2019-01-18-14-48-55	49.9 / 64.2 / 75.3 / 82.4	65.3 / 76.5 / 87.1 / 93.9	59.9 / 75.1 / 84.7 / 92.3	63.2 / 76.8 / 83.6 / 91.5	48.0 / 69.6 / 77.2 / 83.3	- / - / -	61.1 / 73.2 / 84.9 / 91.4	57.7 / 71.0 / 79.4 / 89.8
2019-01-14-12-05-32	49.6 / 60.1 / 72.5 / 82.3	59.7 / 66.2 / 83.5 / 90.8	62.2 / 69.9 / 82.7 / 89.4	56.2 / 69.6 / 81.9 / 90.6	51.4 / 60.1 / 68.4 / 79.4	54.3 / 67.8 / 78.3 / 88.1	- / - / -	59.2 / 68.8 / 79.7 / 91.8
2019-01-17-13-26-38	62.3 / 76.9 / 86.1 / 94.9	62.3 / 69.1 / 81.6 / 90.6	60.8 / 72.9 / 85.7 / 92.0	62.2 / 70.8 / 87.6 / 92.9	45.6 / 66.7 / 74.0 / 80.3	59.1 / 66.1 / 87.1 / 91.4	63.9 / 72.6 / 80.8 / 95.0	59.0 / 61.9 / 81.8 / 91.8
2019-01-18-15-20-12	57.6 / 61.6 / 75.8 / 88.2	60.5 / 78.3 / 88.3 / 93.0	65.2 / 73.8 / 86.2 / 91.9	57.5 / 70.8 / 84.8 / 90.9	45.5 / 59.2 / 66.6 / 75.5	65.9 / 74.4 / 86.8 / 92.8	57.7 / 66.4 / 81.1 / 90.2	56.2 / 70.4 / 81.0 / 89.4
2019-01-10-14-02-34	48.2 / 64.6 / 71.3 / 77.5	62.0 / 75.4 / 82.9 / 91.0	63.6 / 75.5 / 85.9 / 92.6	59.7 / 72.9 / 85.8 / 92.6	48.1 / 63.0 / 67.7 / 79.4	61.4 / 70.0 / 83.0 / 88.4	57.0 / 71.2 / 82.8 / 89.9	55.4 / 69.7 / 78.7 / 85.7
2019-01-14-12-41-24	53.1 / 64.4 / 76.3 / 84.6	54.9 / 66.5 / 80.6 / 92.0	57.2 / 70.5 / 83.8 / 91.6	58.4 / 70.2 / 84.5 / 92.6	52.0 / 65.5 / 68.5 / 82.6	56.0 / 64.6 / 80.1 / 93.4	56.7 / 64.7 / 81.7 / 91.4	58.0 / 64.7 / 82.3 / 90.3
2019-01-15-13-53-14	48.8 / 63.0 / 74.9 / 84.3	59.9 / 76.0 / 87.8 / 94.2	57.1 / 69.9 / 82.1 / 90.8	61.4 / 71.2 / 84.5 / 90.4	48.8 / 65.0 / 70.0 / 82.2	60.9 / 70.5 / 82.8 / 90.2	56.4 / 70.0 / 81.4 / 88.3	60.5 / 68.9 / 8